animals

MDPI

Article

Periostracum Formation in *Sepia officinalis* and *Loligo vulgaris* and Homology with Other Molluscs

Ernesto Ruiz-Villaespesa [1,*], Antonio G. Checa [1], Cristina Lucena-Serrano [2] and Carmen Salas [3]

[1] Departamento de Estratigrafía y Paleontología, Facultad de Ciencias, Universidad de Granada, 18071 Granada, Spain; acheca@ugr.es
[2] Servicios Centrales de Apoyo a la Investigación (SCAI), Universidad de Málaga, 29071 Málaga, Spain
[3] Departamento de Biología Animal, Facultad de Ciencias, Universidad de Málaga, 29071 Málaga, Spain; casanova@uma.es
* Correspondence: rvillaespesa@ugr.es

Simple Summary

In molluscs with external shells, such as gastropods and bivalves, an organic layer known as the periostracum is typically present, covering the outer surface of the mineral shell. The periostracum protects the shell against dissolution and bioerosion and, more importantly, plays a key role during the initial stages of mineralization by acting as both a template for mineral deposition and a barrier to the external environment. This study focuses on the formation of the organic layer in the internal shells of cuttlefish and squid, with the aim of comparing it with periostracum development in other molluscan groups. Using optical microscopy and transmission electron microscopy, we found that both the structure and the mode of formation of these organic layers are similar to those of the periostracum in bivalves and gastropods. Accordingly, their homology can be inferred from morphological criteria.

Abstract

The periostracum is the outermost shell layer and the first produced during shell formation in molluscs. This organic layer isolates the extrapallial space from the external environment and provides a scaffold for subsequent calcification. In cephalopods with an internal shell, some organic shell structures are putatively homologous to the periostracum of other molluscan groups. However, neither their detailed structure nor their mode of formation has been described, leaving the extent of this homology unresolved. To address this issue, we investigated the morphology and formation of the organic layer of the dorsal shield and the gladius in embryos of the cuttlefish *Sepia officinalis* Linnaeus, 1758, and the squid *Loligo vulgaris* Lamarck, 1798, respectively, using light microscopy and transmission electron microscopy. In both species, the periostracum forms within a periostracal groove located along the lateral and anterior margins of the shell sac. As in other molluscs, secretions from columnar cells at the bottom of the groove produce a dense layer, while a translucent layer is subsequently added beneath it through secretions from cuboidal cells. The main difference is the absence of both a pellicle and of the specialized glandular cells that typically secrete it at the bottom of the periostracal groove.

Keywords: periostracum; mollusca; cephalopods; *Sepia officinalis*; cuttlefish; *Loligo vulgaris*; squid

Academic Editors: Blondine Agus and Anna Di Cosmo

Received: 27 January 2026
Revised: 27 February 2026
Accepted: 5 March 2026
Published: 7 March 2026

1. Introduction

The common cuttlefish *Sepia officinalis* Linnaeus, 1758 and the common squid *Loligo vulgaris* Lamarck, 1798 are coleoid cephalopods belonging to the superorder Decapodi-

formes, which is characterized by the presence of ten circumoral appendages. The subclass Coleoidea comprises cephalopods with a reduced internal shell (endocochleate condition) or completely lacking a shell. In contrast, the subclass Nautiloidea includes extant cephalopods with an external shell (ectocochleate condition) and is represented exclusively by the genera *Allonautilus* and *Nautilus* [1,2].

Sepia officinalis and *Loligo vulgaris* are significant commercial species [3–5], and their shells have applications in various fields such as food technology, medicine, and cosmetics [6–12]. The shells of *S. officinalis* (commonly known as the cuttlebone) and *L. vulgaris* (commonly referred to as the gladius or pen) are internal, straight (non-coiled) and elongated structures that function as an internal skeleton providing structural support. However, their differences are noteworthy. Unlike the cuttlebone, the gladius is non-mineralized and lacks chambers. Such differences determine their functional roles and, consequently, the lifestyles of both species. The flexible gladius enhances muscle contractions, thereby improving propulsion and swimming speed, and, due to the absence of chambers, it is not susceptible to collapse under high hydrostatic pressure. On the other hand, the chambered cuttlebone is specialized for buoyancy regulation [13–15].

The composition and structure of both structures have been extensively studied [16–19]. The cuttlebone of *S. officinalis* is composed of calcium carbonate in its aragonite polymorph and contains up to 10% of organic matter, mainly β-chitin and proteins [20,21]. In contrast, the gladius of *L. vulgaris* is entirely organic and consists of nanofibrils of β-chitin crystallites wrapped in α-helical proteins, which self-organize into larger fibres that subsequently assemble into bundles [22].

The cuttlebone is a complex structure composed of two main components: the dorsal shield, which provides skeletal support and protection, and the ventral chamber complex, which contains a balanced mixture of nitrogenous gas and liquid, essential for buoyancy regulation [13]. The dorsal shield consists of three layers: an upper and a lower mineralized layer, and a middle organic layer that extends laterally beyond the margins of the mineralized layers [23,24]. The ventral chambered zone is formed by several horizontal septa supported by vertical pillars. In ventral view, the anterior half is occupied by the last-formed septum, while the posterior half comprises the siphuncular zone, represented by the openings of older chambers [24,25].

The gladius is structurally simpler, consisting of the rachis, a central thickened axis, and the vane, a thin, wide sheath extending along the edges of the posterior rachis [26].

Both the cuttlebone and the gladius are located within the shell sac, a dorsal midline cavity lined by the mantle epithelium, which secretes the materials required for their formation. The morphology of the shell sac epithelium in *S. officinalis* and *L. vulgaris* has been described using light microscopy [27,28] and electron microscopy [23,29,30]. Based on the organization of the shell sac epithelium in *L. vulgaris*, Hopkins & Boletzky [30] proposed that the dorsal and ventral epithelia of the cephalopod shell sac are homologous to the middle and outer mantle folds of other molluscs, respectively. However, they did not observe osmiophilic secretions at the marginal gutter, associated with periostracum formation [30].

The periostracum is an organic layer that covers the outer surface of the mineral shell in molluscs. In bivalves and gastropods, it is secreted within the periostracal groove, located between the middle and outer folds of the mantle edge [31], and represents a key structure in shell formation, as it seals the mineralization compartment and provides a framework upon which the outer shell layer begins to form [31,32]. Moreover, the periostracum protects the shell from dissolution [33] as well as from boring and epizoic organisms [32,34,35].

The formation of the periostracum has been extensively studied in bivalves and some gastropods [31,36,37]. In contrast, periostracum formation has been scarcely described in

cephalopods. To the best of our knowledge, only limited information is available for *Nautilus pompilius* [38] and just a mention in *Spirula spirula* [39]. However, no detailed studies have been conducted on coleoid cephalopods. In this study, we analyze the formation of the middle organic layer of the dorsal shield in *S. officinalis* and the gladius vane in *L. vulgaris*, two structures interpreted as periostracum primarily on the basis of their organic composition, to evaluate their homology with the periostracum of other molluscan groups.

2. Materials and Methods

2.1. Specimen Collection and Fixation

Cuttlefish and squid eggs were collected from egg masses stranded on the shoreline of Estepona, Málaga (South Spain) in April 2023. In the laboratory, the eggs were opened, and embryos at various developmental stages were anesthetized by immersion for 30 min in gradually increasing concentrations of $MgCl_2$ solution up to 3.5%, followed by immediate mechanical destruction of the brain, according to Andrews et al. [40] and Guerra [41] for humane euthanasia. Specimens were then fixed in either 2.5% glutaraldehyde or 4% paraformaldehyde in 0.1 M cacodylate buffer (pH 7.4) for 3 days at 4 °C. The number of specimens analyzed, and the type of analysis performed are indicated in Table 1. *Sepia officinalis* embryos at stages 25, 28 and 30 (pre-hatching), according to Boletzky, Andouche, & Bonnaud-Ponticelli [42] (Figure A1), and *Loligo vulgaris* pre-hatching embryos at stage XIX, according to Naef [43], were processed for this study.

Table 1. Number of specimens of each species used according to type of fixation and analysis.

Species	Fixation	Methacrylate	Alcian Blue-PAS	Calcofluor White	TEM
Sepia officinalis	Glutaraldehyde Paraformaldehyde	2	3	3	4
Loligo vulgaris	Glutaraldehyde Paraformaldehyde		3	3	2

2.2. Methacrylate Embedding

Two undecalcified, paraformaldehyde-fixed *S. officinalis* pre-hatching embryos (stage 30) were embedded in methacrylate at the Andalusian Centre of Nanomedicine and Biotechnology (IBIMA-BIONAND, Malaga, Spain). Samples were dehydrated through an increasing series of ethanol (30, 50, 70, 90 and 100%), embedded in Technovit 7200 VLC (Kulzer Technik; Hanau, Germany), sectioned to a thickness of 50 µm using an EXAKT 300 CP-CL cutting band system (EXAKT; Norderstedt, Germany), and ground with an EXAKT 400 precision microgrinding system (EXAKT; Norderstedt, Germany). Finally, sections were stained with 1% toluidine blue (pH = 8.2) and observed in an Olympus VS120 microscope (Olympus Europe, Hamburg, Germany) at the Central Services for Research (SCAI) of the University of Málaga.

2.3. Transmission Electron Microscopy (TEM)

Two glutaraldehyde-fixed *S. officinalis* embryos at stage 25, two at stage 28, and two at stage 30, as well as two glutaraldehyde-fixed prehatching *L. vulgaris* embryos, were decalcified in 4% EDTA, post-fixed in 1% OsO_4 for 1 h, and contrasted with 2% uranyl acetate overnight at room temperature in the dark. Samples were then dehydrated through an increasing series of acetone and embedded in Spurr resin (Electronic Microscopy Science-Biolyst; Morgantown, PA, USA). Sections were obtained using a Leica EM UC7/FC7 ultramicrotome (Leica; Wetzlar, Germany). Semithin sections of 0.5 µm were stained with 1% toluidine blue and observed using an Olympus VS120 optical microscope. Ultrathin

sections of 70 nm were collected on Formvar-coated copper grids and examined by transmission electron microscopy using a JEOL-JEM1400 (JEOL Ltd., Tokyo, Japan) located at the SCAI of the University of Málaga.

2.4. Alcian Blue– Periodic Acid–Schiff Staining

Alcian Blue (AB) combined with Periodic Acid–Schiff (PAS) staining was employed to distinguish acidic polysaccharides, which stain blue, from neutral polysaccharides, which stain purple to pink [44].

Three paraformaldehyde-fixed pre-hatching embryos from each species were decalcified in 4% EDTA and subsequently embedded in paraffin. Microtome sections (8 µm thick) were deparaffinized in xylene, rehydrated through a decreasing ethanol series, and sequentially stained with 1% Alcian Blue (pH 2.5) for 30 min. Sections were then oxidized with 0.5% periodic acid for 10 min, incubated with Schiff's reagent for 30 min in the dark and counterstained with Carazzi's hematoxylin for 5 min. Distilled water rinses were performed between each step. Stained sections were dehydrated through an increasing ethanol series, cleared in eucalyptol and xylene, and mounted in DPX mounting medium.

2.5. Calcofluor White Assay

Paraffin sections (8 µm thick) of paraformaldehyde-fixed prehatching embryos from both species were first deparaffinized in xylene and hydrated through an increasing series of ethanol. Sections were then incubated in the dark at room temperature with Calcofluor White (CFW 18909 Sigma-Aldrich; Darmstadt, Germany) at a final concentration of 0.05% for 5 min, to label β-linked polysaccharides (e.g., chitin and cellulose). After staining, samples were rinsed in distilled water to remove excess dye and mounted in Mowiol 4–88 (Sigma-Aldrich; Darmstadt, Germany). Labelled sections were imaged using a Leica Stellaris 8 confocal microscope ((Leica; Wetzlar, Germany) at the SCAI of the University of Málaga, using excitation and emission wavelengths of 405 nm and 420–476 nm, respectively.

3. Results

The lumen of the shell sac in *Sepia officinalis* (Figure 1A) and *Loligo vulgaris* (Figure 1G) was narrower at the anterior and lateral margins, forming grooves from which the periostracum emerged. The periostracum thickened progressively from the bottom of the groove toward the longitudinal axis of the shell sac (Figure 1B,E–I). In *S. officinalis*, the periostracal groove was ventrally concave (Figure 1B,D–F), whereas in *L. vulgaris* it remained straight (Figure 1G–I). The first mineralization of the dorsal shield in *S. officinalis* appeared beneath the periostracum at the most distal end of the periostracal groove, just before it opened into the lumen of the shell sac (Figure 1C).

In AB–PAS–stained sections, the periostracum exhibited magenta (PAS–positive) staining in both species (Figure 1D,G), which is consistent with the presence of neutral polysaccharides. In *Sepia officinalis*, AB–positive blue staining was detected at the bottom of the periostracal groove (arrow in Figure 1D), indicating the presence of acidic polysaccharides. Calcofluor White (CFW) fluorescence was detected throughout the periostracum in both *S. officinalis* (Figure 1E) and *L. vulgaris* (Figure 1G).

As observed with TEM, the bottom of the periostracal groove in both species was lined ventrally by columnar epithelial cells and dorsally by squamous cells (Figure 2A,D). At its innermost part, the periostracal groove was closed by cells, referred to here as "bottom cells", whose apical plasma membranes exhibited microvilli oriented perpendicular to those of the cells of the dorsal and ventral epithelia. *Sepia officinalis* possessed a single curved bottom cell (Figure 2A), whereas *Loligo vulgaris* had two bottom cells, one dorsal and one ventral (Figure 2D,E).

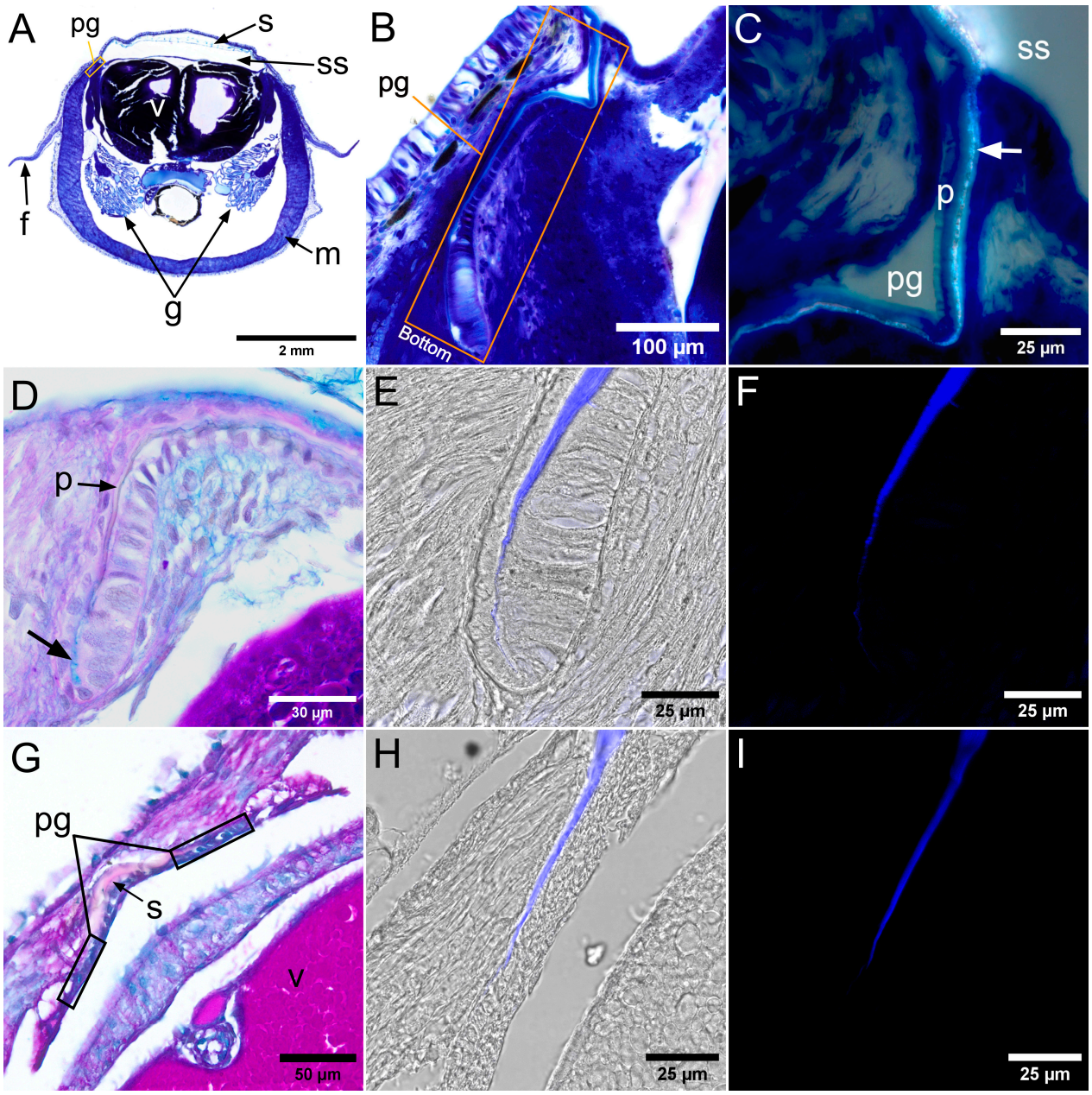

Figure 1. Undecalcified methacrylate (**A**–**C**) and decalcified paraffin (**D**–**I**) transverse sections of pre-hatching *Sepia officinalis* (**A**–**F**) and *Loligo vulgaris* (**G**–**I**). (**A**–**C**) Methacrylate transverse sections of *S. officinalis* stained with Toluidine Blue. (**A**) The lumen of the shell sac (ss) occupies the dorsal region and contains the shell (s). The periostracal groove (pg) is located at the margins of the shell sac (frame). (**B**) Detail of the ventrally concave periostracal groove (pg). The periostracum thickens along its narrow lumen. (**C**) Polarized light microscopy image revealing incipient mineralization of the dorsal shield (arrow) beneath the organic periostracum (p). (**D**) Transverse section through the bottom of the periostracal groove in *S. officinalis* stained with AB–PAS. AB-positive secretions are visible at the bottom of the periostracal groove (thick arrow), while the recently formed periostracum (p) is PAS–positive. (**E**,**F**) Transverse section through the periostracal groove in *S. officinalis* stained with CFW. Blue fluorescence is observed along the periostracum. Panel (**E**) is an overlay of the brightfield and the fluorescence image shown in (**F**). (**G**) Transverse section through the dorsum of *L. vulgaris* stained with AB–PAS. The shell (s) is PAS-positive and the periostracal groove (pg) extends laterally. (**H**,**I**) Transverse section through the periostracal groove in *L. vulgaris* stained with CFW. Blue fluorescence is observed along the periostracum. Panel (**H**) is an overlay of the brightfield and the fluorescence image showed in (**I**). f, lateral fin; g, gills; m, musculature; p, periostracum; pg, periostracal groove; s, shell; ss, shell sac; v, vitelum.

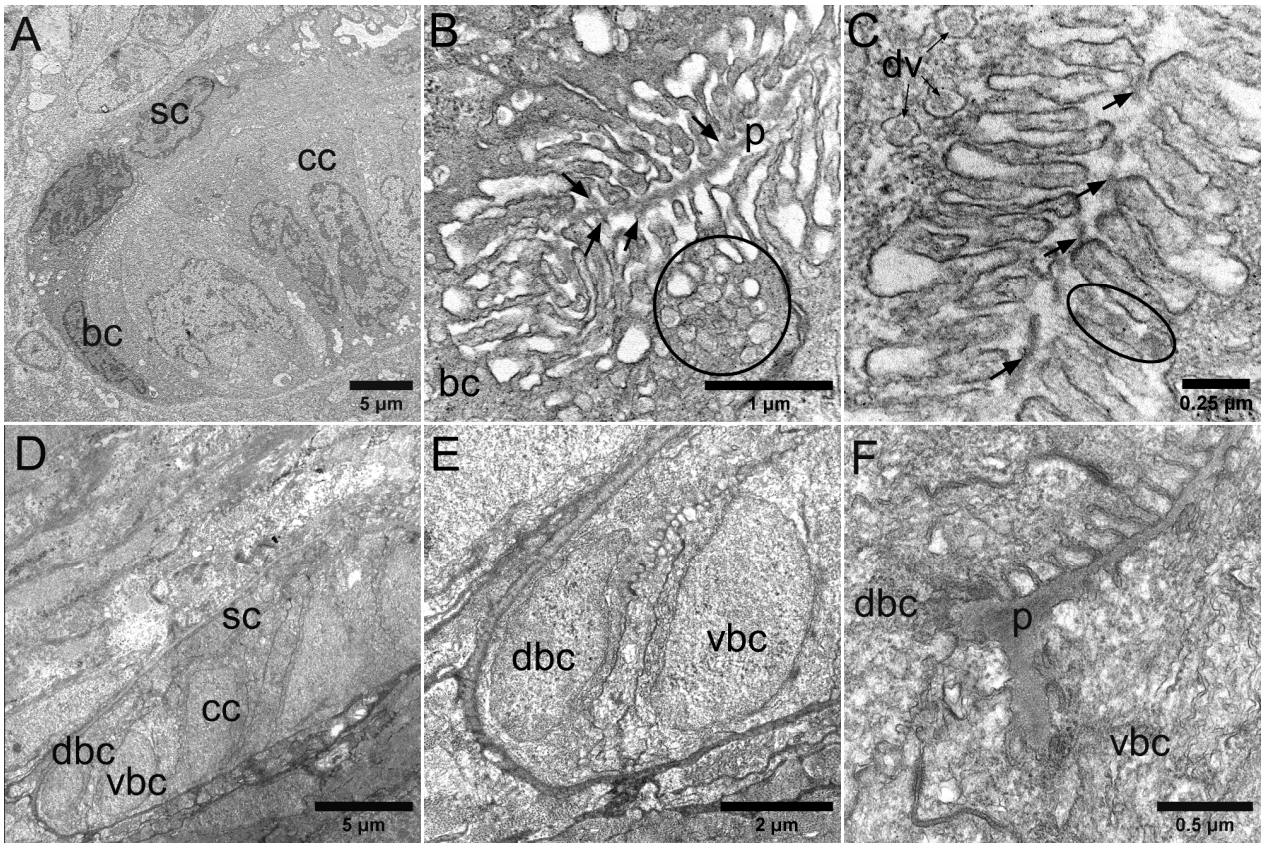

Figure 2. TEM images showing the bottom of the periostracal groove in *Sepia officinalis* at stage 28 (**A**–**C**) and pre-hatching *Loligo vulgaris* (**D**–**F**). (**A**) Epithelium at the bottom of the periostracal groove in *S. officinalis.* (**B**) Closed end of the lumen of the periostracal groove. Electron-dense vesicles are observed undergoing exocytosis in a ventral epithelial cell (outline) and others being incorporated into the periostracum (arrows). (**C**) Periostracum units (arrows) aligned within the confined lumen, between the microvilli of the epithelial cells. Membrane-bound electron-dense vesicles are visible inside a dorsal cell, while rounded electron-dense material is secreted by a ventral cell (outline). (**D**) Epithelium at the bottom of the periostracal groove in *L. vulgaris*. (**E**) Magnified view of the bottom cells. (**F**) Electron-dense periostracum (p) formed at the closed end of the lumen of the periostracal groove. bc, bottom cell; cc, columnar cell; dbc, dorsal bottom cell; dv, electron-dense vesicle; p, periostracum; sc, squamous cell; v, vesicles; vbc, ventral bottom cell.

The periostracum was formed by electron-dense secretions deposited within the lumen of the periostracal groove (Figure 2B,C,F). Numerous electron-dense vesicles were observed in cells at the bottom of the periostracal groove, some undergoing exocytosis (outlined regions in Figure 2B,C) and others likely being incorporated into the periostracum (arrows in Figure 2B). In *S. officinalis*, discrete periostracal units were occasionally observed between the microvilli of the dorsal and ventral epithelial cells (arrows in Figure 2C).

Progressing upward along the periostracal groove of *Sepia officinalis* secretions increased and comprised small vesicles, large vacuoles, and multilamellar bodies (Figure 3A). The periostracum became progressively thicker (Figure 3A,B). Dorsal cells displayed short, loosely arranged microvilli, with no detectable secretory activity (Figure 3B). In contrast, secretions continued from the ventral cells, which transitioned from columnar to cuboidal and displayed elongated, straight microvilli forming a brush border (Figure 3B,C). Electron-dense vesicles were also observed, albeit in lower numbers compared with those found in cells at the bottom. Further along, fibres developed beneath the dense periostracal layer (Figure 3C), later organizing into a fibrous translucent layer (Figure 3D). At the interspace

between the microvilli of the ventral epithelium and the most recently formed fibres of the translucent layer, electron-dense material was observed (Figure 3D).

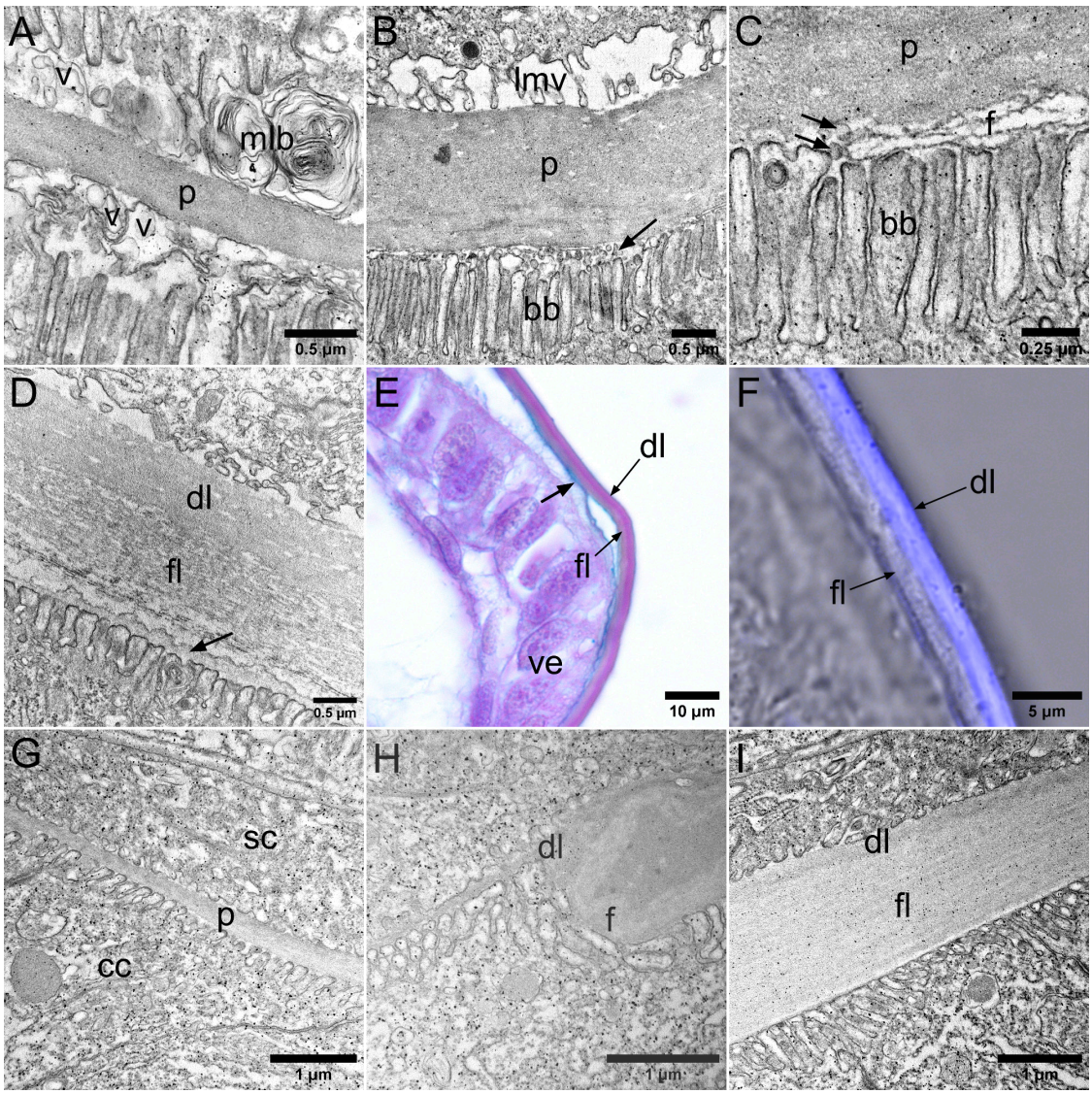

Figure 3. TEM (**A**–**D**,**G**–**I**) and light microscopy (**E**,**F**) images showing the periostracum along the periostracal groove in *Sepia officinalis* (stage 28) (**A**–**F**) and pre-hatching *Loligo vulgaris* (**G**–**I**). (**A**) The periostracum (p) at the bottom of the periostracal groove consists of a dense layer. Secretions from both epithelia include vesicles (v) and multilamellar bodies (mlb). (**B**) The periostracum (p) thickens progressively along the periostracal groove. The ventral epithelium exhibits a brush border with straight, closely packed microvilli (bb), whereas the dorsal epithelium shows loosely arranged microvilli (lmv). Numerous vesicles are secreted by the ventral epithelium (arrow). (**C**) Fibres (f) develop beneath the periostracum (p), with some vesicles still visible (arrows). (**D**) A translucent fibrous layer (fl) develops beneath the dense layer (dl). Note the electron-dense material filling the space between the brush border of the ventral epithelium and the most recently formed fibre (arrow). (**E**) In AB–PAS-stained sections, the dense layer (dl) stains strongly magenta (PAS–positive), while the translucent fibrous layer (fl) shows minimal staining. Between the ventral epithelium (ve) and the translucent layer, some fibres stain blue (AB–positive). (**F**) CFW fluorescence is observed in the dense layer (dl) but not in the fibrous translucent layer (fl). (**G**) Periostracal groove in *L. vulgaris*. The dense periostracal layer (p) lies between dorsal squamous cells (sc) and ventral columnar cells (cc). (**H**) A sudden thickening of the periostracum occurs, apparently resulting from the folding of the translucent fibrous layer onto itself, (f) beneath the dense layer (dl). (**I**) A translucent fibrous layer (fl) develops beneath the thin dense layer (dl).

The staining affected the two layers differently. The dense layer was strongly stained by both PAS (Figure 3E) and CFW (Figure 3F), whereas the translucent layer showed little to no reaction. In AB–PAS-stained sections, blue AB-positive staining was also observed beneath the translucent layer (Figure 3E).

In *Loligo vulgaris*, the dense periostracal layer showed no appreciable increase in thickness along the periostracal groove (Figure 3G–I). The periostracum underwent a sudden thickening (Figure 3H), giving rise to a densely fibrous translucent layer below the thin dense layer (Figure 3I).

In pre-hatching embryos of *Sepia officinalis* (stage 30), the large size of the specimens required embedding of a smaller fragment. Sectioning of the specimens resulted in detachment of the periostracum, disrupting its natural spatial relationship with the epithelium (Figure 4A). Numerous vesicles and vacuoles secreted by the ventral epithelium were observed either deposited on the surface of the translucent layer or trapped within it (Figure 4A–C). These appeared to be largely produced by highly vacuolated cells of the distal ventral epithelium (Figure 4A), which contributed to the formation of the fibrous translucent layer (Figure 4B,C). Vortices of nanolaminae were observed in the dense layer (thick arrows in Figure 4B,C), which also appeared more fibrous (Figure 4C). At the bottom of the periostracal groove, columnar cells were shorter and fully loaded with electron-dense vesicles (Figure 4D).

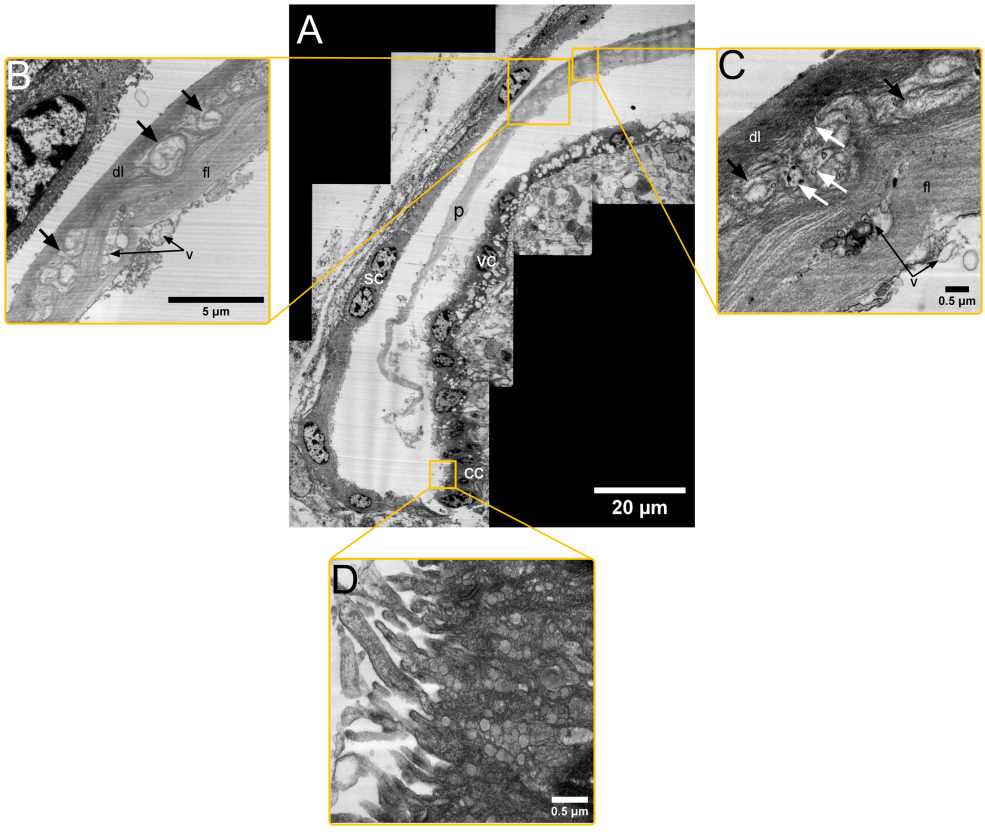

Figure 4. Periostracal groove of *Sepia officinalis* at stage 30. (**A**) The epithelium is composed ventrally of a row of columnar cells (cc) at the bottom of the periostracal groove, and wider cuboidal vacuolated cells (vc) at its distal end; dorsally, it consists of flat squamous cells (sc). The periostracum (p) extends within the periostracal groove cavity. (**B**,**C**) The dense layer (dl) contains multiple vortices (black arrows), while the translucent layer (fl) contains numerous vesicles and vacuoles (v) either trapped within it or attached to its surface. Some vesicles are also visible inside the vortices of the dense layer (white arrows in (**C**)). (**D**) Detail of the columnar cells, which exhibit long microvilli and contain numerous electron-dense vesicles.

4. Discussion

In coleoid cephalopods, the periostracum has been occasionally mentioned, primarily in terms of its organic composition and its development prior to calcification, thus enabling shell extension [15,45,46]. However, its formation process and structure remained unstudied. In this study, a detailed account of periostracum formation in *Loligo vulgaris* and *Sepia officinalis* is provided. Here, we examine its main characteristics and compare them with those described in other molluscs to assess their potential homology. Our model for periostracum formation in *S. officinalis* and *L. vulgaris* is illustrated in Figure 5. The main features in both species compared to other molluscs are summarized in Table 2.

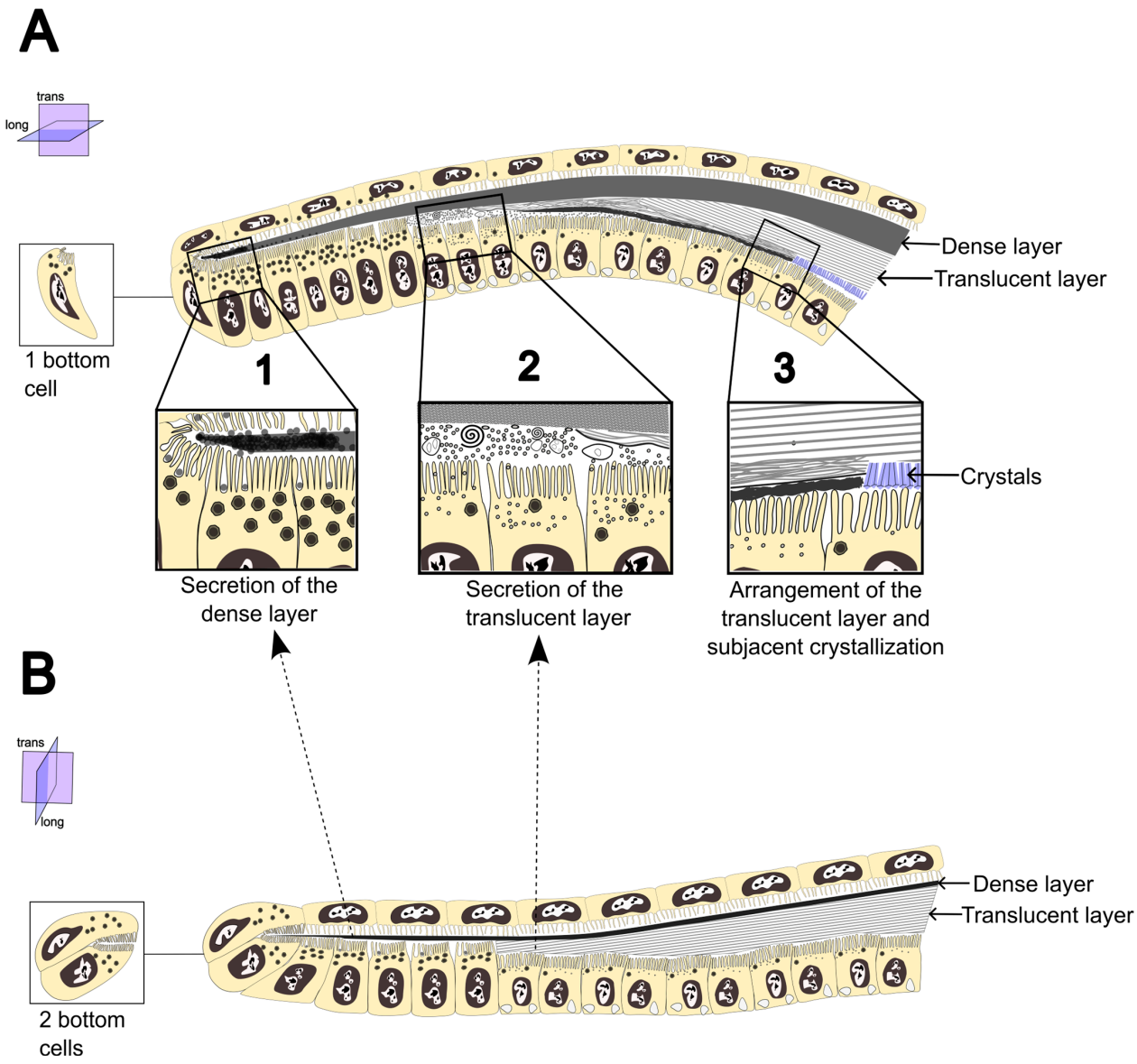

Figure 5. Schematic model illustrating periostracum formation in *Sepia officinalis* (**A**) and *Loligo vulgaris* (**B**). (**1**). Formation of the dense layer at the bottom of the periostracal groove mainly from secretions of ventral columnar cells. (**2**) Formation of the fibrous translucent layer from secretions of ventral cuboidal cells. (**3**) Arrangement of the translucent layer and subsequent mineralization beneath it, only in *S. officinalis*.

Table 2. Main morphological features of periostracum formation in *Sepia officinalis* and *Loligo vulgaris*, compared with those reported in bivalves and gastropods.

	Sepia officinalis	*Loligo vulgaris*	Bivalves and Gastropods
Shape of the periostracal groove	Ventrally curved	Straight	Ventrally coiled
Bottom cells	One single curved cell with microvilli	Two cells (one dorsal and one ventral) with microvilli	Basal cell/s (bivalves) or gland cells (gastropods) secreting a pellicle
Periostracal layers	A dense layer and a translucent layer	A (thinner) dense layer and a translucent layer	A dense layer and a (transitional) translucent layer
Secretory epithelium	Columnar and cuboidal (ventral shell sac)	Columnar and cuboidal (ventral shell sac)	Columnar (inner side of the outer mantle fold)

As in bivalves and gastropods, in the cephalopods *S. officinalis* and *L. vulgaris* the periostracum develops within a narrow periostracal groove. In the former groups, the periostracal groove is located between the middle and outer folds of the mantle edge, whereas in the studied cephalopods it is found at the lateral and anterior edges of the shell sac. According to Hopkins and Boletzky [30], the ventral epithelium of the shell sac edges, composed of columnar and cuboidal cells, corresponds to the inner surface of the outer mantle fold, while the dorsal epithelium, composed of flattened squamous cells, corresponds to the outer surface of the middle fold. In *L. vulgaris*, the periostracal groove is straight relative to the shell sac (Figure 1G–I), whereas in *S. officinalis* it bends ventrally (Figures 1B, 2D–F and 4A) (compare Figure 5A,B; Table 2). This latter condition is common among bivalves, in which the periostracal groove undergoes a pronounced coiling toward the inner surface of the outer fold of the mantle edge [31,37]. Both *S. officinalis* and *L. vulgaris* lack glandular cells lying below the epithelium, such as those commonly present in gastropods [37]. The innermost cells of the periostracal groove, although exhibiting slightly different morphologies from adjacent cells (Figures 2A,D,E and 5), do not display typical characteristics of bivalve basal cells, such as the absence of microvilli and a highly folded apical plasma membrane [31]. Furthermore, they do not secrete a pellicle. To distinguish them from bivalve basal cells, we hereafter refer to them as "bottom cells" (Table 2).

The columnar cell row, restricted to a narrow band of the ventral epithelium at the base of the periostracal groove, appears to be primarily responsible for secreting the dense layer, which constitutes the first-formed layer of the periostracum (Figures 2B,C,F, 3A–C,G–I and 4A). In these columnar cells, numerous electron-dense vesicles are present (Figures 2B, 4D and 5). Although such vesicles can occur in other cells of the periostracal groove, their pronounced abundance in the columnar cells at the bottom suggests a primary role in the formation of the dense layer. In the bivalve *Acila insignis*, identical electron-dense vesicles are secreted into the periostracum by the inner epithelium of the outer mantle fold [47]. Similar electron-dense vesicles, derived from the Golgi apparatus, have also been reported in gastropods, where they are presumed to serve as precursors of the periostracum [36,48].

Beneath the dense layer, the translucent layer is formed from secretions of cuboidal cells of the ventral epithelium (Figures 3B–F,H,I, 4A–C and 5). In bivalves, the dense layer is thought to form via sclerotization of the translucent layer [49] with the dense layer increasing in thickness at the expense of the translucent layer, which becomes thinner. In *S. officinalis* and *L. vulgaris*, however, no such thickening of the dense layer via sclerotization of the translucent layer was observed. Instead, the fibres of the translucent layer appear to become more compact without forming a new dense layer (Figures 3D,I and 4A–C). In

the distal region of the periostracal groove, the dense and translucent layers each occupy about half of the periostracum, with the dense layer dorsal and the translucent layer ventral (Figure 4A–C) This distribution is also evident in AB–PAS and CFW staining, in which the dense layer stains intensely, while the translucent layer shows minimal staining (Figure 3E,F). In *L. vulgaris*, the dense layer remains notably thin after formation of the translucent layer (Figure 3G–I), which then occupies nearly the entire periostracum and exhibits highly aligned fibres (Figure 3I).

5. Conclusions

Both the organic layer of the dorsal shield in *Sepia officinalis* and the gladius of *Loligo vulgaris* form within a narrow groove at the edges of the mantle, consisting of a dense layer secreted by ventral columnar cells and a subjacent translucent layer secreted by ventral cuboidal cells. Despite differences, such as the secretion of a pellicle by basal cells, their formation and morphology are comparable to that of the periostracum in bivalves and gastropods, and they can thus be considered true periostraca.

Author Contributions: Conceptualization, E.R.-V., C.S. and A.G.C.; methodology, E.R.-V. and C.L.-S.; investigation, E.R.-V.; formal analysis, E.R.-V.; resources, C.S. and A.G.C.; data curation, E.R.-V.; writing—original draft preparation, E.R.-V.; writing—review and editing, C.S. and A.G.C.; visualization, E.R.-V.; supervision, C.S. and A.G.C.; project administration, C.S. and A.G.C.; funding acquisition, C.S. and A.G.C. All authors have read and agreed to the published version of the manuscript.

Funding: E.R.-V., C.S. and A.G.C. acknowledge projects PID2023-146394NB-I00 funded by the Spanish Ministry of Science, Innovation and Universities (MICIU/AEI/10.13039/501100011033) and by ERDF (EU), and PCM 00092 (Consejería de Economía, Innovación, Ciencia y Empleo, Junta de Andalucía). E.R.-V. was supported by a pre-doctoral FPU grant (FPU20/05502) from the Spanish Ministry of Science, Innovation and Universities. Funding for open access charge was partly provided by Universidad de Granada/CBUA.

Institutional Review Board Statement: Not applicable.

Informed Consent Statement: Not applicable.

Data Availability Statement: All data are available from the corresponding author upon reasonable request.

Acknowledgments: We thank Juan F. López Téllez for performing some TEM procedures and Alejandro Domínguez Moreno for preparing methacrylate sections, both using equipment provided by the ICTS "NANBIOSIS", specifically the U28-Nanoimaging Unit at IBIMA Plataforma BIONAND. We also thank Francisco David Navas Fernández (SCAI, Universidad de Málaga) for assistance with confocal microscopy. E.R.-V. and A.G.C. further acknowledge Research Group RNM363 (Consejería de Economía, Innovación, Ciencia y Empleo, Junta de Andalucía), and the Unidad Científica de Excelencia UCE-PP2016-05 (University of Granada). C.S. acknowledges Research Group RNM 141 (Consejería de Economía, Innovación, Ciencia y Empleo, Junta de Andalucía).

Conflicts of Interest: The authors declare no conflicts of interest.

Appendix A

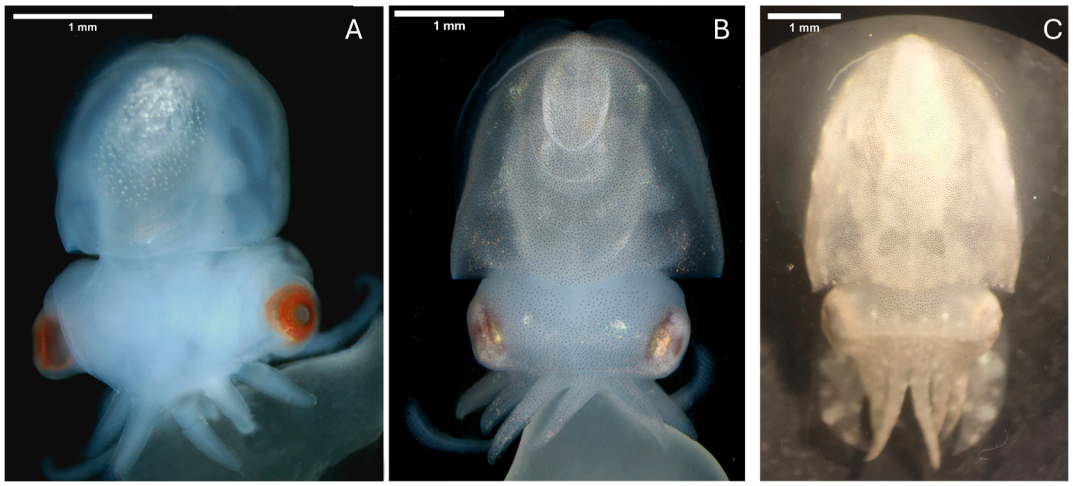

Figure A1. *Sepia officinalis* embryos at stage 25 (**A**), 28 (**B**) and 30 (**C**).

References

1. Lindgren, A.R.; Giribet, G.; Nishiguchi, M.K. A Combined Approach to the Phylogeny of Cephalopoda (Mollusca). *Cladistics* **2004**, *20*, 454–486. [CrossRef]
2. WoRMS—World Register of Marine Species. Available online: https://www.marinespecies.org (accessed on 9 January 2026).
3. Arkhipkin, A.I.; Rodhouse, P.G.K.; Pierce, G.J.; Sauer, W.; Sakai, M.; Allcock, L.; Arguelles, J.; Bower, J.R.; Castillo, G.; Ceriola, L.; et al. World Squid Fisheries. *Rev. Fish. Sci. Aquac.* **2015**, *23*, 92–252. [CrossRef]
4. Hastie, L.C.; Pierce, G.J.; Wang, J.; Bruno, I.; Moreno, A.; Piatkowski, U.; Robin, J.P. Cephalopods in the North-Eastern Atlantic: Species, Biogeography, Ecology, Exploitation and Conservation. In *Oceanography and Marine Biology*, 1st ed.; CRC Press: Raton, FL, USA, 2016; Volume 47, ISBN 9781420094220.
5. Jereb, P.; Roper, C.F.E.; Vecchione, M. Introduction. In *Cephalopods of the World. An Annotated and Illustrated Catalogue of Species Known to Date. Chambered Nautiluses and Sepioids (Nautilidae, Sepiidae, Sepiolidae, Sepiadariidae, Idiosepiidae and Spirulidae)*, 4th ed.; Jereb, P., Roper, C.F.E., Eds.; FAO Species Catalogue for Fishery Purposes: Rome, Italy, 2005; Volume 1, ISBN 9251053839.
6. Cadman, J.; Zhou, S.; Chen, Y.; Li, Q. Cuttlebone: Characterisation, Application and Development of Biomimetic Materials. *J. Bionic Eng.* **2012**, *9*, 367–376. [CrossRef]
7. Youn, D.K.; No, H.K.; Prinyawiwatkul, W. Preparation and Characteristics of Squid Pen β-Chitin Prepared under Optimal Deproteinisation and Demineralisation Condition. *Int. J. Food Sci. Technol.* **2013**, *48*, 571–577. [CrossRef]
8. Hajji, S.; Younes, I.; Ghorbel-Bellaaj, O.; Hajji, R.; Rinaudo, M.; Nasri, M.; Jellouli, K. Structural Differences between Chitin and Chitosan Extracted from Three Different Marine Sources. *Int. J. Biol. Macromol.* **2014**, *65*, 298–306. [CrossRef]
9. Olsen, R.L.; Toppe, J.; Karunasagar, I. Challenges and Realistic Opportunities in the Use of By-Products from Processing of Fish and Shellfish. *Trends Food Sci. Technol.* **2014**, *36*, 144–151. [CrossRef]
10. Abdelmalek, B.E.; Sila, A.; Haddar, A.; Bougatef, A.; Ayadi, M.A. β-Chitin and Chitosan from Squid Gladius: Biological Activities of Chitosan and Its Application as Clarifying Agent for Apple Juice. *Int. J. Biol. Macromol.* **2017**, *104*, 953–962. [CrossRef]
11. Nisticò, R. Aquatic-Derived Biomaterials for a Sustainable Future: A European Opportunity. *Resources* **2017**, *6*, 65. [CrossRef]
12. Carvalho, D.N.; Gonçalves, C.; Sousa, R.O.; Reis, R.L.; Oliveira, J.M.; Silva, T.H. Extraction and Purification of Biopolymers from Marine Origin Sources Envisaging Their Use for Biotechnological Applications. *Mar. Biotechnol.* **2024**, *26*, 1079–1119. [CrossRef]
13. Denton, E.J.; Gilpin-Brown, J.B. The Buoyancy of the Cuttlefish, *Sepia officinalis* (L.). *J. Mar. Biol. Assoc. UK* **1961**, *41*, 319–342. [CrossRef]
14. Denton, J.E. On Buoyancy and the Lives of Modern and Fossil Cephalopods. *Proc. R. Soc. London. Ser. B Biol. Sci.* **1974**, *185*, 273–299. [CrossRef]
15. Arkhipkin, A.I.; Bizikov, V.A.; Fuchs, D. Vestigial Phragmocone in the Gladius Points to a Deepwater Origin of Squid (Mollusca: Cephalopoda). *Deep. Sea Res. Part I Oceanogr. Res. Pap.* **2012**, *61*, 109–122. [CrossRef]
16. Le Pabic, C.; Marie, A.; Marie, B.; Percot, A.; Bonnaud-Ponticelli, L.; Lopez, P.J.; Luquet, G. First Proteomic Analyses of the Dorsal and Ventral Parts of the *Sepia officinalis* Cuttlebone. *J. Proteom.* **2017**, *150*, 63–73. [CrossRef] [PubMed]
17. Le Pabic, C.; Derr, J.; Luquet, G.; Lopez, P.J.; Bonnaud-Ponticelli, L. Three-Dimensional Structural Evolution of the Cuttlefish *Sepia officinalis* Shell from Embryo to Adult Stages. *J. R. Soc. Interface* **2019**, *16*, 20190175. [CrossRef] [PubMed]

18. Messerli, M.A.; Raihan, M.J.; Kobylkevich, B.M.; Benson, A.C.; Bruening, K.S.; Shribak, M.; Rosenthal, J.J.C.; Sohn, J.J. Construction and Composition of the Squid Pen from *Doryteuthis pealeii*. *Biol. Bull.* **2019**, *237*, 1–15. [CrossRef]
19. Dauphin, Y.; Luquet, G.; Percot, A.; Bonnaud-Ponticelli, L. Comparison of Embryonic and Adult Shells of *Sepia officinalis* (Cephalopoda, Mollusca). *Zoomorphology* **2020**, *139*, 151–169. [CrossRef]
20. Birchall, J.D.; Thomas, N.L. On the Architecture and Function of Cuttlefish Bone. *J. Mater. Sci.* **1983**, *18*, 2081–2086. [CrossRef]
21. Florek, M.; Fornal, E.; Gómez-Romero, P.; Zieba, E.; Paszkowicz, W.; Lekki, J.; Nowak, J.; Kuczumow, A. Complementary Microstructural and Chemical Analyses of *Sepia officinalis* Endoskeleton. *Mater. Sci. Eng. C* **2009**, *29*, 1220–1226. [CrossRef]
22. Yang, F.C.; Peters, R.D.; Dies, H.; Rheinstädter, M.C. Hierarchical, Self-Similar Structure in Native Squid Pen. *Soft Matter* **2014**, *10*, 5541–5549. [CrossRef]
23. Bandel, K.; Boletzky, S. A Comparative Study of the Structure, Development and Morphological Relationships of Chambered Cephalopod Shells. *Veliger* **1979**, *21*, 313–354.
24. Griesshaber, E.; Checa, A.G.; Salas, C.; Hoffmann, R.; Yin, X.; Neuser, R.; Rupp, U.; Schmahl, W.W. Biological Light-Weight Materials: The Endoskeletons of Cephalopod Mollusks. *J. Struct. Biol.* **2023**, *215*, 107988. [CrossRef] [PubMed]
25. Checa, A.G.; Cartwright, J.H.E.; Sánchez-Almazo, I.; Andrade, J.P.; Ruiz-Raya, F. The Cuttlefish *Sepia officinalis* (Sepiidae, Cephalopoda) Constructs Cuttlebone from a Liquid-Crystal Precursor. *Sci. Rep.* **2015**, *5*, 11513. [CrossRef]
26. Donovan, D.T.; Toll, R.B. The Gladius in Coleoid (Cephalopoda) Evolution. In *Paleontology and Neontology of Cephalopods*; Clarke, M.R., Trueman, E.R., Eds.; Academic Press, Inc.: London, UK, 1988; Volume 12.
27. Appellöf, J. Die Schalen von Sepia, Spirula Und Nautilus: Studien Über Den Bau Und Das Wachsthum. In *Kungliga Svenska Vetenskapsakademiens Handlingar*; Nordstedt & Söner, P.A.: Stockholm, Sweden, 1893; Volume 25.
28. Spiess, P.E. Organogenese Des Schalendrusenkomplexes Bei Einigen Coleoiden Cephalopoden Des Mittlemeeres. *Rev. Suisse Zool.* **1972**, *79*, 167–226.
29. Kawaguti, S.; Oda, A. Electron Microscopy on the Cuttlebone-Producing Cells. *Biol. J. Okayama Univ.* **1963**, *9*, 41–53.
30. Hopkins, B.; Boletzky, S. The Fine Morphology of the Shell Sac in the Squid Genus *Loligo* (Mollusca: Cephalopoda): Features of a Modified Conchiferan Program. *Veliger* **1994**, *37*, 344–357.
31. Checa, A.; Salas, C. Periostracum and Shell Formation in the Bivalvia. In *Treatise Online*; Paleontological Institute of the University of Kansas: Lawrence, Kansas, 2017; Volume 1, pp. 1–51.
32. Clark, G.R. Shell Growth in the Marine Environment: Approaches to the Problem of Marginal Calcification. *Integr. Comp. Biol.* **1976**, *16*, 617–626. [CrossRef]
33. Tevesz, M.J.S.; Carter, J.G. *Environmental Relationships of Shell Form and Structure of Unionacean Bivalves*; Springer: New York, NY, USA, 1980; pp. 295–322. [CrossRef]
34. Bottjer, D.J. Periostracum of the Gastropod *Fusitriton oregonensis*: Natural Inhibitor of Boring and Encrusting Organisms. *Bull. Mar. Sci.* **1981**, *31*, 916–921.
35. Harper, E.M. The Molluscan Periostracum: An Important Constraint in Bivalve Evolution. *Palaeontology* **1997**, *40*, 71–91.
36. Bevelander, G.; Nakahara, H. An Electron Microscope Study of the Formation and Structure of the Periostracum of a Gastropod, *Littorina littorea*. *Calcif. Tissue Res.* **1970**, *5*, 1–12. [CrossRef]
37. Saleuddin, A.S.M.; Petit, H.P. The Mode of Formation and the Structure of the Periostracum. *Mollusca* **1983**, *4*, 199–234. [CrossRef]
38. Westermann, B.; Schmidtberg, H.; Beuerlein, K. Functional Morphology of the Mantle of *Nautilus pmpilius* (Mollusca, Cephalopoda). *J. Morphol.* **2005**, *264*, 277–285. [CrossRef]
39. Checa, A.G.; Grenier, C.; Griesshaber, E.; Schmahl, W.W.; Cartwright, J.H.E.; Salas, C.; Oudot, M. The Shell Structure and Chamber Production Cycle of the Cephalopod *Spirula* (Coleoidea, Decabrachia). *Mar. Biol.* **2022**, *169*, 132. [CrossRef]
40. Andrews, P.L.R.; Darmaillacq, A.S.; Dennison, N.; Gleadall, I.G.; Hawkins, P.; Messenger, J.B.; Osorio, D.; Smith, V.J.; Smith, J.A. The Identification and Management of Pain, Suffering and Distress in Cephalopods, Including Anaesthesia, Analgesia and Humane Killing. *J. Exp. Mar. Biol. Ecol.* **2013**, *447*, 46–64. [CrossRef]
41. Guerra, Á. Functional Anatomy: Macroscopic Anatomy and Post-Mortem Examination. In *Handbook of Pathogens and Diseases in Cephalopods*; Gestal, C., Pascual, S., Guerra, Á., Fiorito, G., Vieites, J., Eds.; Springer: Cham, Switzerland, 2019; pp. 11–38, ISBN 9783030113308.
42. Boletzky, S.; Andouche, A.; Bonnaud-Ponticelli, L. A Developmental Table of Embryogenesis in *Sepia officinalis*. *Vie Milieu* **2016**, *66*, 11–23.
43. Naef, A. *Die Cephalopoden (Embryologie), Fauna e Flora Del Golfo Di Napoli*; Bardi, G., Friedlander, R.S., Eds.; Stazione Zoologica di Napoli: Naples, Italy, 1928; Volume 2, pp. 1–35.
44. Roth, J.; Taatjes, D.J. Histochemistry and Cell Biology-a Glance into the Past and a Look Ahead. *Histochem. Cell Biol.* **2023**, *159*, 465–475. [CrossRef]
45. Bandel, K. Cephalopod Shell Structure and General Mechanisms of Shell Formation. In *Skeletal Biomineralization: Patterns, Processes and Evolutionary Trends*; Carter, J.G., Ed.; American Geophysical Union: Washington, DC, USA, 1989; Volume 5, pp. 97–115.

46. Fuchs, D.; Keupp, H.; Mitta, V.; Engeser, T. Ultrastructural Analyses on the Conotheca of the Genus *Belemnotheutis* (Belemnitida: Coleoidea). In *Cephalopods Present and Past: New Insights and Fresh Perspectives*; Landman, N.H., Davis, R.A., Mapes, R.H., Eds.; Springer: Dordrecht, The Netherlands, 2007; pp. 299–314.
47. Salas, C.; Bueno-Pérez, J.d.D.; López-Téllez, J.F.; Checa, A.G. Form and Function of the Mantle Edge in Protobranchia (Mollusca: Bivalvia). *Zoology* **2022**, *153*, 126027. [CrossRef]
48. Saleuddin, A.S.M. An Electron Microscopic Study on the Formation of the Periostracum in *Helisoma* (Mollusca). *Calcif. Tissue Res.* **1975**, *18*, 297–310. [CrossRef] [PubMed]
49. Salas, C.; Marina, P.; Checa, A.G.; Rueda, J.L. The Periostracum of *Digitaria digitaria* (Bivalvia: Astartidae): Formation and Structure. *J. Molluscan Stud.* **2012**, *78*, 34–43. [CrossRef]